NANO LETTERS

Letter

pubs.acs.org/NanoLett

Parametric Resonance of Magnetization Excited by Electric Field

Yu-Jin Chen,*[,†] Han Kyu Lee,[†] Roman Verba,[‡] Jordan A. Katine,[¶] Igor Barsukov,[†] Vasil Tiberkevich,[§] John Q. Xiao,[∥] Andrei N. Slavin,[§] and Ilya N. Krivorotov[†]

[†]Department of Physics and Astronomy, University of California, Irvine, California 92697, United States

[‡]Institute of Magnetism, Kyiv 03142, Ukraine

[¶]HGST, San Jose, California 95135, United States

[§]Department of Physics, Oakland University, Rochester, Michigan 48309, United States

[∥]Department of Physics and Astronomy, University of Delaware, Newark, Delaware 19716, United States

Supporting Information

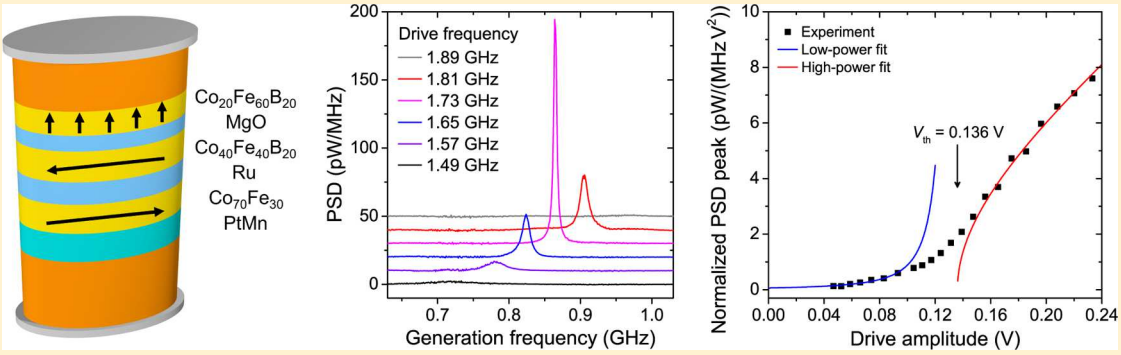

ABSTRACT: Manipulation of magnetization by electric field is a central goal of spintronics because it enables energy-efficient operation of spin-based devices. Spin wave devices are promising candidates for low-power information processing, but a method for energy-efficient excitation of short-wavelength spin waves has been lacking. Here we show that spin waves in nanoscale magnetic tunnel junctions can be generated via parametric resonance induced by electric field. Parametric excitation of magnetization is a versatile method of short-wavelength spin wave generation, and thus, our results pave the way toward energy-efficient nanomagnonic devices.

KEYWORDS: *Parametric resonance, voltage-controlled magnetic anisotropy, spin waves, magnetic tunnel junction*

Magneto-electric coupling in magnetic materials and heterostructures enables control of magnetization by electric field, which is the key requirement for realization of energy-efficient spintronic devices.[1] Recent progress in this field includes demonstration of electric field induced magnetization reversal[2−8] and ferromagnetic resonance.[9,10] However, ferromagnetic resonance driven by electric field cannot be used for generation of spin waves with wavelengths smaller than the excitation region, which limits its applicability in nanomagnonic devices based on short-wavelength spin waves.[11] Here we report parametric excitation of spin waves in a ferromagnet by alternating electric field. Unlike ferromagnetic resonance, parametric resonance can be employed for generation and amplification of short-wavelength spin waves, and thus, our work is an important step toward the development of energy-efficient nanomagnonics.

A prominent manifestation of the magneto-electric coupling in magnetic films and heterostructures is modification of magnetic anisotropy by electric field.[12−14] This recently discovered effect takes place at the interface between a ferromagnetic metal (e.g., Fe) and a nonmagnetic insulator (e.g., MgO)[14] and originates from different rates of filling of *d*-like electron bands in response to electric field applied perpendicular to the interface.[15] Since electrons in different bands contribute unequally to the uniaxial perpendicular magnetic anisotropy (PMA) at the interface, electric field can be used to modulate PMA. This voltage-controlled magnetic anisotropy (VCMA) is promising for energy-efficient manipulation of magnetization[4,16,17] because, unlike spin torque (ST), VCMA does not rely on high electric current density resulting in large Ohmic losses. In this work, we employ VCMA modulation at microwave frequencies in order to excite parametric resonance of magnetization in a nanomagnet.[18−20]

Parametric excitation of magnetization by external magnetic field has been thoroughly studied in bulk and thin-film ferromagnets.[21] In these experiments, a parameter of the magnetic system (external field) is modulated with a frequency at twice a spin wave frequency f_{SW} of the system. Parametric

Received: November 11, 2016
Revised: December 20, 2016
Published: December 21, 2016

DOI: 10.1021/acs.nanolett.6b04725
Nano Lett. 2017, 17, 572−577

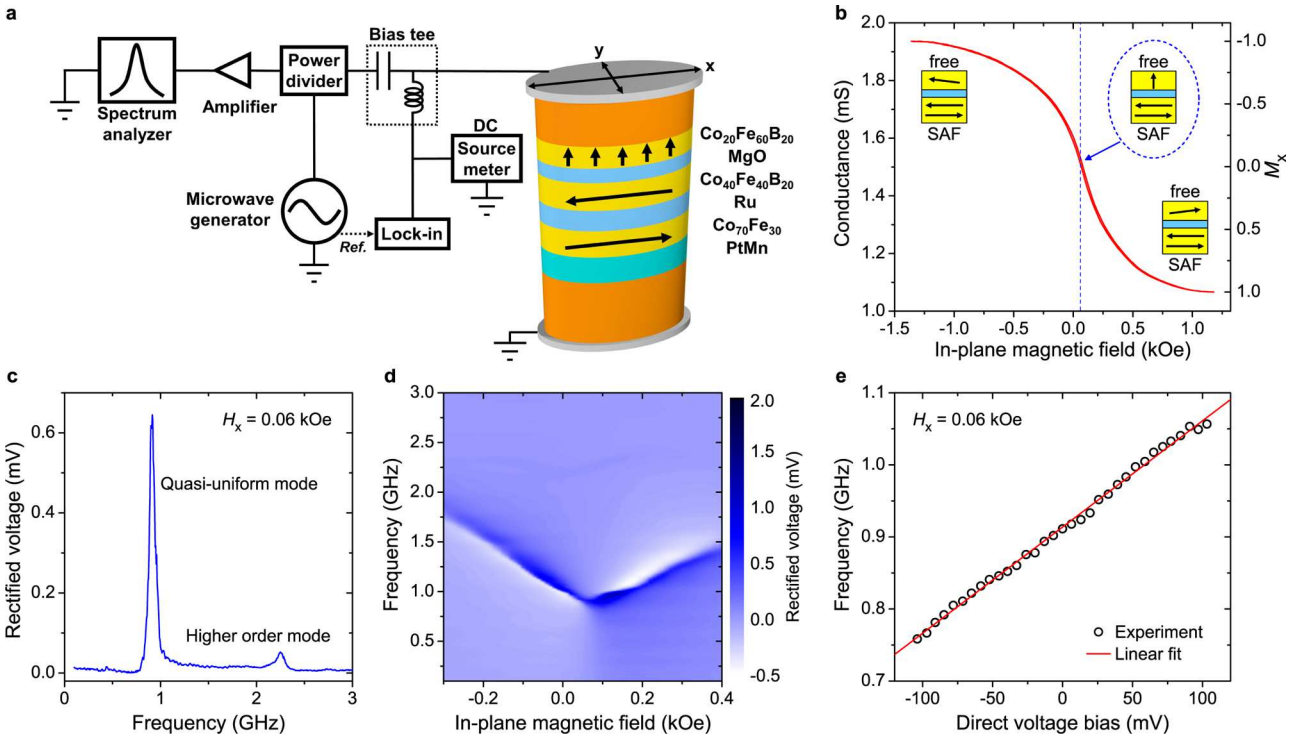

Figure 1. Measurement setup and MTJ characterization. (a) Schematic of experimental setup for DC and microwave characterization of MTJ. (b) MTJ conductance as a function of in-plane magnetic field H_x applied parallel to the MTJ long axis. (c) ST-FMR spectrum of the MTJ at H_x = 0.06 kOe. (d) Dependence of ST-FMR spectra on H_x. (e) Quasi-uniform mode frequency versus direct voltage bias V_{dc} measured at H_x = 0.06 kOe.

excitation is a nonlinear process, in which the parametric drive acts as negative effective magnetic damping that competes with positive intrinsic damping.[21] At a threshold amplitude of the parametric drive, the negative damping exceeds the intrinsic damping and magnetization oscillations at half the drive frequency are excited.

Parametric excitation of magnetization has several important advantages over direct excitation by external magnetic field with a frequency at f_{SW}. First, parametric excitation efficiently couples not only to the uniform precession of magnetization but also to spin wave eigenmodes.[21] This allows excitation of short-wavelength spin waves by simply choosing the parametric drive frequency to be twice the desired spin wave frequency. Second, parametric pumping can be used for frequency-selective amplification of spin waves[22] and phase error corrections.[23] All these properties of parametric pumping form a highly desirable set of tools for the nascent field of nanomagnonics.[24,25] However, parametric excitation of spin waves by microwave magnetic field in metallic ferromagnets is not energy-efficient because of the relatively high threshold fields (tens of Oe).[26] Here we show that replacing magnetic field pumping by electric field (VCMA) pumping solves this problem and allows parametric excitation of magnetic oscillations in metallic ferromagnets by a low-power microwave drive.

We demonstrate parametric excitation of magnetization in 70 nm × 150 nm elliptical nanoscale magnetic tunnel junctions (MTJs) schematically shown in Figure 1a. The junctions are patterned from (bottom lead)/Ta(5)/PtMn(15)/SAF/$MgO(0.83)/Co_{20}Fe_{60}B_{20}(1.58)$/Ta(5)/(cap) multilayers (thicknesses in nm) deposited by magnetron sputtering. Here SAF = $Co_{70}Fe_{30}(2.3)/Ru(0.85)/Co_{40}Fe_{40}B_{20}(2.4)$ is the pinned synthetic antiferromagnet, which has magnetic moments lying in the plane of the sample. The equilibrium direction of the $Co_{20}Fe_{60}B_{20}$ free layer magnetization is normal to the sample plane due to interfacial PMA.[10] Prior to patterning, the multilayers are annealed for 2 h at 300 °C in a 10 kOe in-plane magnetic field that sets the pinned layer exchange bias direction parallel to the MTJ long axis.

All measurements reported in this Letter are made in the setup schematically shown in Figure 1a that allows application of DC and microwave voltages to the MTJ and measurement of DC and microwave signals generated by the MTJ. Figure 1b shows conductance G of the MTJ measured as a function of in-plane magnetic field H_x applied parallel to the MTJ long axis. The shape of the $G(H_x)$ curve is congruent to the shape of the $M_x(H_x)$ hysteresis loop,[10] where M_x is normalized projection of the free layer magnetization onto the applied field direction. The hysteresis loop and micromagnetic simulations confirm the out-of-plane easy axis of the free layer (see Supporting Information Section 1). The center of the loop is shifted from zero field due to a residual 0.06 kOe stray field from the SAF.

We employ spin torque ferromagnetic resonance (ST-FMR) to characterize the spectral properties of spin wave eigenmodes of the MTJ. In this technique, a small amplitude microwave drive current $GV_{ac}\sin(2\pi f_d t)$ applied to the MTJ excites oscillations of magnetization at the drive frequency f_d. The resulting resistance oscillations $R_{ac}\sin(2\pi f_d t + \phi)$ of the MTJ at the drive frequency lead to partial rectification of the microwave drive voltage V_{ac} and generate a direct voltage V_r. Peaks in ST-FMR spectra $V_r(f_d)$ arise from resonant excitation of spin wave eigenmodes of the MTJ.[27,28]

Figure 1c shows a ST-FMR spectrum of the MTJ measured at H_x = 0.06 kOe. Two spin wave eigenmodes are present in this spectrum with the lowest-frequency (f_{SW} = 0.91 GHz)

DOI: 10.1021/acs.nanolett.6b04725
Nano Lett. 2017, 17, 572−577

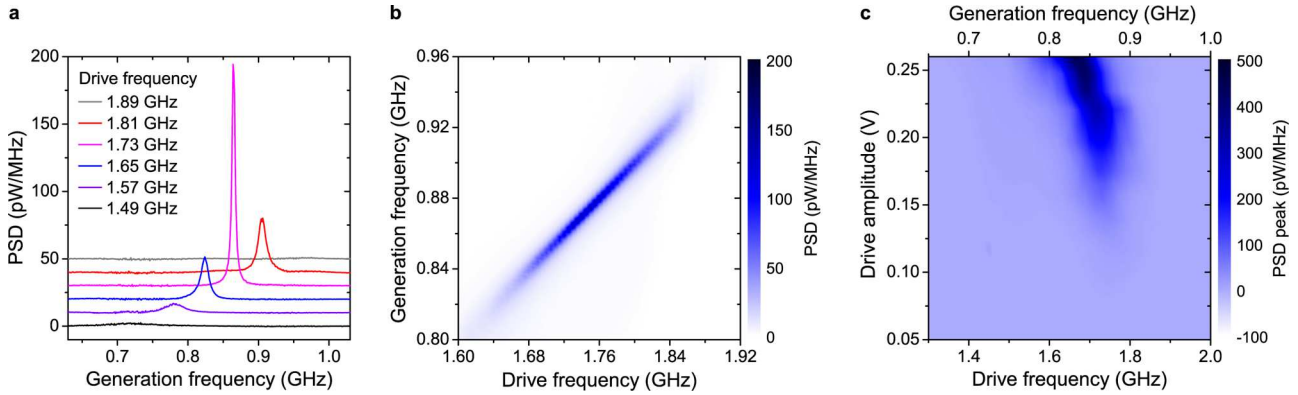

Figure 2. Parametric resonance. (a) Power spectral density (PSD) of the microwave signal emitted by the MTJ under VCMA parametric drive of V_{ac} = 0.185 V. Curves are vertically offset for clarity and are listed in order of drive frequency. (b) Dependence of the parametrically generated emission spectra on the drive frequency for V_{ac} = 0.185 V. (c) PSD peak plotted versus drive frequency and drive amplitude reveals typical Arnold tongue shape characteristic of parametric excitation.

mode being the quasi-uniform mode of the free layer.[29] From the spectral line width of the quasi-uniform mode we can estimate the Gilbert damping parameter $\alpha \approx 0.033$ (see Supporting Information Section 2), which is typical for a CoFeB layer of this thickness.[10] Dependence of ST-FMR spectra on H_x is summarized in Figure 1d. The frequency of the quasi-uniform mode increases with increasing absolute value of the net in-plane field due to the second-order uniaxial PMA.[10]

Figure 1e shows dependence of the quasi-uniform mode frequency on direct voltage bias V_{dc} applied to the MTJ. From the slope of the line in Figure 1e we can estimate VCMA efficiency $\frac{dH_u}{dV_{dc}} = 526$ Oe/V (see Supporting Information Section 3), where H_u is the PMA field and the value of VCMA efficiency is typical for this material system.[10]

We use the parallel pumping geometry to parametrically excite the free layer quasi-uniform mode[18] in which magnetization of the free layer is parallel to the oscillating PMA field H_u. We apply a constant 0.06 kOe in-plane magnetic field along the long axis of the ellipse to compensate the in-plane SAF stray field acting on the free layer so that its magnetization is aligned perpendicular to the sample plane. We then apply a parametric drive voltage V_{ac} to the MTJ and vary the drive frequency f_d about $2f_{SW}$ (twice the quasi-uniform mode resonance frequency). The resulting modulation of PMA at the drive frequency due to VCMA can parametrically excite magnetization oscillations at half the drive frequency,[18] which gives rise to the MTJ resistance oscillations $R_{ac}\cos\left(2\pi\frac{f_d}{2}t + \phi\right)$. These resistance oscillations can be detected via their mixing with the microwave current $GV_{ac}\cos(2\pi f_d t)$ through the junction, which generates mixing voltage signals $V_{mix}(t)$ at frequencies $f_d/2$ and $3f_d/2$:

$$V_{mix}(t) = GV_{ac}\cos(2\pi f_d t)R_{ac}\cos\left(2\pi\frac{f_d}{2}t + \phi\right)$$
$$= \frac{1}{2}GV_{ac}R_{ac}\left[\cos\left(2\pi\frac{f_d}{2}t - \phi\right) + \cos\left(2\pi\frac{3f_d}{2}t + \phi\right)\right] \quad (1)$$

As illustrated in Figure 1a, we amplify $V_{mix}(t)$ and measure its spectrum with a microwave spectrum analyzer. In this Letter, we present power spectra of $V_{mix}(t)$ measured near $f_d/2$; similar spectra are observed near $3f_d/2$. Figure 2a displays power spectral density (PSD) $P(f)$ of $V_{mix}(t)$ measured at several fixed values of the drive frequency f_d near $2f_{SW}$ and drive amplitude V_{ac} = 0.185 V. The maximum of each power spectrum is observed exactly at $f_d/2$, clearly illustrating that magnetization dynamics of the free layer is excited parametrically at half the drive frequency. The line widths of the measured spectral peaks are in the range of several MHz. This line width mostly arises from thermal fluctuations of the free layer magnetization (fluctuations of the phase ϕ in eq 1). Figure 2b illustrates that parametric excitation of the quasi-uniform mode has well-pronounced resonant character: significant amplitude of the parametric oscillations is observed only in a narrow range of the drive frequencies near $2f_{SW}$.

Figure 2c displays dependence of $P(f_d/2)$ on the drive amplitude V_{ac} and drive frequency f_d. This figure illustrates the parametric excitation efficiency and clearly demonstrates that the observed microwave emission from the sample has a threshold character in V_{ac}. This threshold behavior is expected for parametric resonance that is excited when effective negative damping from the parametric drive exceeds the positive natural damping of the excited mode.[21] Figure 2c also shows that the parametric resonance frequency f_{pr} (defined as f_d that gives maximum $P(f_d/2)$ at a given value of V_{ac}) shifts to lower values with increasing drive amplitude due to nonlinear frequency shift, as expected for a uniaxial ferromagnet.[21] The shape of the parametric instability region in Figure 2c is a typical Arnold tongue of a nonlinear parametric oscillator.[30]

In order to quantitatively determine the threshold drive voltage V_{th} needed to excite parametric resonance of the quasi-uniform mode, we analyze reduced power of this mode p as a function of the drive amplitude V_{ac}. By definition, $p = |c|^2$ where c is dimensionless amplitude of the quasi-uniform mode (see Supporting Information Section 4), which is proportional to the amplitude of the MTJ resistance oscillations, so that $p \approx (GR_{ac})^2$. It is clear from eq 1 that PSD of the reduced power $p(f)$ is proportional to $P(f)/V_{ac}^2$ for any V_{ac}. In Figure 3, we plot its resonant value $P(f_{pr}/2)/V_{ac}^2$, which is proportional to $p(f_{pr}/2)$, as a function of V_{ac}.

Analytical expressions for $p(f_{pr}/2)$ can be derived in the limit of $V_{ac} \ll V_{th}$. In this limit, magnetization dynamics are small-amplitude thermal fluctuations amplified by the parametric drive, for which

DOI: 10.1021/acs.nanolett.6b04725
Nano Lett. 2017, 17, 572−577

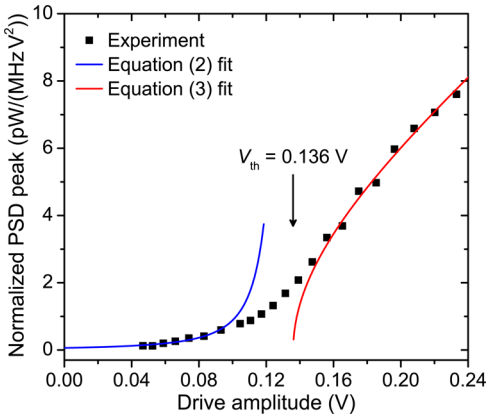

Figure 3. Parametric resonance threshold. Normalized peak amplitude of PSD, $P(f_{pr}/2)/V_{ac}^2$, measured at parametric resonance as a function of the parametric drive amplitude V_{ac}. Best fits of eqs 2 and 3 to the data (solid lines) give the parametric resonance threshold voltage V_{th} = 0.136 V.

$$p(f_{pr}/2) = \frac{A}{(V_{th} - V_{ac})^2} \quad (2)$$

where A is a constant (see Supporting Information Section 5).

In the opposite limit of $V_{ac} \gg V_{th}$, thermal fluctuations can be neglected and the following analytical expression for the reduced power p can be derived by

$$p = B\sqrt{V_{ac}^2 - V_{th}^2} \quad (3)$$

where B is a constant (see Supporting Information Section 5).

For our system, p in eq 3 can be replaced by $p(f_{pr}/2)$ because the measured spectral line width of $P(f)$ at $f_d = f_{pr}$ depends weakly on V_{ac} for $V_{ac} > 0.16$ V. Therefore, we can fit the data in Figure 3 using eq 2 in the small amplitude limit and eq 3 in the large amplitude limit. The best fit shown by the blue (small amplitude) and red (large amplitude) lines in Figure 3 gives V_{th} = 0.136 V. In this fitting procedure, A and B are free fitting parameters, while V_{th} is treated as a common fitting parameter for both the small and large amplitude limits (see Supporting Information Section 5).

It is instructive to compare the measured V_{th} to its theoretically expected value for our MTJ geometry and the measured VCMA efficiency (see Supporting Information Section 4). The calculated threshold voltage in the macrospin approximation is V_{th} = 0.086 V, while that given by micromagnetic simulations is V_{th} = 0.156 V. The measured value is similar to the micromagnetic prediction, which lends support to VCMA origin of the observed parametric resonance.

In our experiment, spin-polarized tunneling current flows through the MTJ, which results in ST and Oersted field acting on the free layer. However, these types of drive play a negligible role in exciting parametric resonance compared to the VCMA drive. The Oersted field has nearly circular symmetry, and therefore, it poorly couples to the quasi-uniform mode. The effective fields of both the field-like and damping-like ST lie in the sample plane, which corresponds to perpendicular pumping geometry. Parametric excitation of the quasi-uniform mode at $f_d = 2f_{SW}$ is inefficient in this geometry.[21]

Our experiment employs MTJ magnetic configuration with in-plane SAF and out-of-plane free layer that is convenient for unambiguous demonstration and quantitative analysis of parametric resonance excited by VCMA. However, we find that VCMA-driven parametric resonance can be observed in other types of MTJ configurations. Figure 4 shows out-of-plane

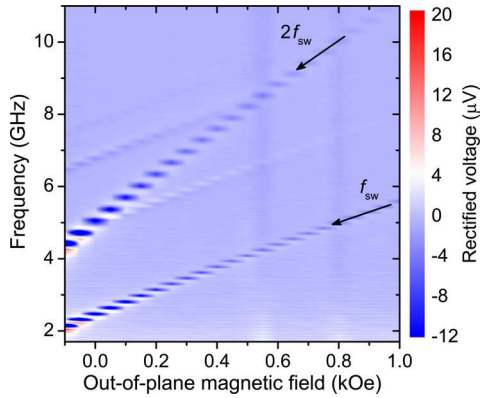

Figure 4. Parametric resonance in ST-FMR. ST-FMR spectra of an MTJ with out-of-plane SAF and free layers measured as a function of out-of-plane magnetic field. Resonance at twice the quasi-uniform mode frequency arises from parametric excitation of the quasi-uniform mode.

magnetic field dependence of ST-FMR spectra measured for a 30 nm × 95 nm MTJ with out-of-plane equilibrium configuration of both the free and SAF layers. Owing to the smaller amplitude of the rectified voltage in this collinear geometry, we employ ultrasensitive ST-FMR with magnetic field modulation[29] rather than conventional ST-FMR with amplitude modulation.

The ST-FMR spectra measured at a large value of the microwave drive voltage V_{ac} = 0.4 V reveal several spin wave eigenmodes of the free layer. Another prominent resonance is observed at twice the frequency of the lowest-frequency (quasi-uniform) spin wave eigenmode. In this collinear MTJ geometry, the microwave resistance oscillations of the device have a significant component at twice the excited spin wave mode frequency and mix with the parametric drive at twice the mode frequency to give rise to a rectified voltage peak at $2f_{SW}$ measured by ST-FMR. The amplitude of this additional resonance at $2f_{SW}$ relative to the amplitude of the resonance at f_{SW} increases with increasing V_{ac}, which is a signature of a thermally smeared threshold behavior similar to that in Figure 3. The out-of-plane collinear geometry is commonly employed in ST magnetic memory (STT-MRAM), and parametric resonance signals in ST-FMR of STT-MRAM can potentially be used for characterization of the free layer properties such as magnetic damping.

While magnetic damping in ultrathin films of metallic ferromagnets is significant, signal processing devices based on spin wave propagation in nanowires made from these films are feasible if short-wavelength spin waves are employed.[18] The group velocities of such exchange-dominated spin waves can be sufficiently high to enable micrometer-scale spin wave propagation. For example, we calculate the decay length of a 0.1 μm wavelength spin wave in a 1 nm thick, 100 nm wide Fe/MgO nanowire to be 2 μm, assuming the damping constant α = 0.004[31] and the spin wave dispersion appropriate for the nanowire.[18] This decay length is sufficiently long to enable signal propagation between neighboring spin wave logic gates separated by submicrometer distances.[32] Furthermore, large VCMA at the Fe/MgO interface[14] can be employed for

DOI: 10.1021/acs.nanolett.6b04725
Nano Lett. 2017, 17, 572−577

parametric amplification of spin waves propagating between the gates to counteract the spin wave amplitude decay.[33]

In summary, our work shows that magneto-electric coupling can be used to excite parametric resonance of magnetization by electric field. We employ voltage-controlled magnetic anisotropy at the CoFeB/MgO interface to excite parametric oscillations of a CoFeB free layer magnetization in nanoscale magnetic tunnel junctions. The threshold voltage for parametric excitation in this system is found to be well below 1 V, which is attractive for applications in energy-efficient spintronic and magnonic nanodevices such as spin wave logic.[34] This work opens a new energy-efficient route for excitation of magnetization dynamics in thin films of metallic ferromagnets and nanodevices based on magnetic multilayers.

■ ASSOCIATED CONTENT

Supporting Information

The Supporting Information is available free of charge on the ACS Publications website at DOI: 10.1021/acs.nanolett.6b04725.

Micromagnetic simulations of the ground state of the MTJ, estimate of the Gilbert damping, estimate of the VCMA efficiency, theoretical calculation of the parametric resonance threshold, and details of evaluating the parametric resonance threshold in experiment (PDF)

■ AUTHOR INFORMATION

Corresponding Author

*E-mail: yujin.chen@uci.edu.

ORCID

Yu-Jin Chen: 0000-0002-3006-7308

Author Contributions

Y.-J.C., H.K.L., and R.V. contributed equally to this work. Y.-J.C. and H.K.L. performed electrical characterization of the MTJ samples. J.A.K. made the samples. R.V., V.T., and A.N.S. developed the theoretical model. I.N.K., A.N.S., I.B., and J.Q.X. formulated the experimental and theoretical approaches. I.N.K. and A.N.S. managed the project. All authors analyzed the data and cowrote the paper.

Notes

The authors declare no competing financial interest.

■ ACKNOWLEDGMENTS

We acknowledge the Center for NanoFerroic Devices (CNFD) and the Nanoelectronics Research Initiative (NRI) for funding of this work. This work was also supported by NSF Grants EFMA-1641989, ECCS-1309416, ECCS-1305586, and DMR-1610146, by DTRA Grant HDTRA1-16-1-0025, and by the FAME Center, one of six centers of STARnet, an SRC program sponsored by MARCO and DARPA.

■ REFERENCES

(1) Matsukura, F.; Tokura, Y.; Ohno, H. *Nat. Nanotechnol.* **2015**, *10*, 209−220.

(2) Chiba, D.; Yamanouchi, M.; Matsukura, F.; Ohno, H. *Science* **2003**, *301*, 943−945.

(3) Baek, S. H.; Jang, H. W.; Folkman, C. M.; Li, Y. L.; Winchester, B.; Zhang, J. X.; He, Q.; Chu, Y. H.; Nelson, C. T.; Rzchowski, M. S.; Pan, X. Q.; Ramesh, R.; Chen, L. Q.; Eom, C. B. *Nat. Mater.* **2010**, *9*, 309−314.

(4) Shiota, Y.; Nozaki, T.; Bonell, F.; Murakami, S.; Shinjo, T.; Suzuki, Y. *Nat. Mater.* **2012**, *11*, 39−43.

(5) Cuellar, F. A.; Liu, Y. H.; Salafranca, J.; Nemes, N.; Iborra, E.; Sanchez-Santolino, G.; Varela, M.; Garcia Hernandez, M.; Freeland, J. W.; Zhernenkov, M.; Fitzsimmons, M. R.; Okamoto, S.; Pennycook, S. J.; Bibes, M.; Barthélémy, A.; te Velthuis, S. G. E.; Sefrioui, Z.; Leon, C.; Santamaria, J. *Nat. Commun.* **2014**, *5*, 4215.

(6) Heron, J. T.; Trassin, M.; Ashraf, K.; Gajek, M.; He, Q.; Yang, S. Y.; Nikonov, D. E.; Chu, Y.-H.; Salahuddin, S.; Ramesh, R. *Phys. Rev. Lett.* **2011**, *107*, 217202.

(7) He, X.; Wang, Y.; Wu, N.; Caruso, A. N.; Vescovo, E.; Belashchenko, K. D.; Dowben, P. A.; Binek, C. *Nat. Mater.* **2010**, *9*, 579−585.

(8) Bauer, U.; Yao, L.; Tan, A. J.; Agrawal, P.; Emori, S.; Tuller, H. L.; van Dijken, S.; Beach, G. S. D. *Nat. Mater.* **2015**, *14*, 174−181.

(9) Nozaki, T.; Shiota, Y.; Miwa, S.; Murakami, S.; Bonell, F.; Ishibashi, S.; Kubota, H.; Yakushiji, K.; Saruya, T.; Fukushima, A.; Yuasa, S.; Shinjo, T.; Suzuki, Y. *Nat. Phys.* **2012**, *8*, 491−496.

(10) Zhu, J.; Katine, J. A.; Rowlands, G. E.; Chen, Y.-J.; Duan, Z.; Alzate, J. G.; Upadhyaya, P.; Langer, J.; Khalili Amiri, P.; Wang, K. L.; Krivorotov, I. N. *Phys. Rev. Lett.* **2012**, *108*, 197203.

(11) Yu, H.; d' Allivy Kelly, O.; Cros, V.; Bernard, R.; Bortolotti, P.; Anane, A.; Brandl, F.; Heimbach, F.; Grundler, D. *Nat. Commun.* **2016**, *7*, 11255.

(12) Weisheit, M.; Fähler, S.; Marty, A.; Souche, Y.; Poinsignon, C.; Givord, D. *Science* **2007**, *315*, 349−351.

(13) Chiba, D.; Sawicki, M.; Nishitani, Y.; Nakatani, Y.; Matsukura, F.; Ohno, H. *Nature* **2008**, *455*, 515−518.

(14) Maruyama, T.; Shiota, Y.; Nozaki, T.; Ohta, K.; Toda, N.; Mizuguchi, M.; Tulapurkar, A. A.; Shinjo, T.; Shiraishi, M.; Mizukami, S.; Ando, Y.; Suzuki, Y. *Nat. Nanotechnol.* **2009**, *4*, 158−161.

(15) Niranjan, M. K.; Duan, C.-G.; Jaswal, S. S.; Tsymbal, E. Y. *Appl. Phys. Lett.* **2010**, *96*, 222504.

(16) Wang, W.-G.; Li, M.; Hageman, S.; Chien, C. L. *Nat. Mater.* **2012**, *11*, 64−68.

(17) Schellekens, A. J.; van den Brink, A.; Franken, J. H.; Swagten, H. J. M.; Koopmans, B. *Nat. Commun.* **2012**, *3*, 847.

(18) Verba, R.; Tiberkevich, V.; Krivorotov, I.; Slavin, A. *Phys. Rev. Appl.* **2014**, *1*, 044006.

(19) Kurebayashi, H.; Dzyapko, O.; Demidov, V. E.; Fang, D.; Ferguson, A. J.; Demokritov, S. O. *Appl. Phys. Lett.* **2011**, *99*, 162502.

(20) Manuilov, S. A.; Du, C. H.; Adur, R.; Wang, H. L.; Bhallamudi, V. P.; Yang, F. Y.; Hammel, P. C. *Appl. Phys. Lett.* **2015**, *107*, 042405.

(21) Gurevich, A. G.; Melkov, G. A. *Magnetization Oscillations and Waves*; CRC Press: Boca Raton, FL, 1996.

(22) Melkov, G. A.; Kobljanskyj, Y. V.; Serga, A. A.; Tiberkevich, V. S.; Slavin, A. N. *Phys. Rev. Lett.* **2001**, *86*, 4918.

(23) Chumak, A. V.; Vasyuchka, V. I.; Serga, A. A.; Kostylev, M. P.; Tiberkevich, V. S.; Hillebrands, B. *Phys. Rev. Lett.* **2012**, *108*, 257207.

(24) Kruglyak, V. V.; Demokritov, S. O.; Grundler, D. *J. Phys. D: Appl. Phys.* **2010**, *43*, 264001.

(25) Chumak, A. V.; Vasyuchka, V. I.; Serga, A. A.; Hillebrands, B. *Nat. Phys.* **2015**, *11*, 453−461.

(26) Urazhdin, S.; Tiberkevich, V.; Slavin, A. *Phys. Rev. Lett.* **2010**, *105*, 237204.

(27) Tulapurkar, A. A.; Suzuki, Y.; Fukushima, A.; Kubota, H.; Maehara, H.; Tsunekawa, K.; Djayaprawira, D. D.; Watanabe, N.; Yuasa, S. *Nature* **2005**, *438*, 339−342.

(28) Sankey, J. C.; Braganca, P. M.; Garcia, A. G. F.; Krivorotov, I. N.; Buhrman, R. A.; Ralph, D. C. *Phys. Rev. Lett.* **2006**, *96*, 227601.

(29) Gonçalves, A. M.; Barsukov, I.; Chen, Y.-J.; Yang, L.; Katine, J. A.; Krivorotov, I. N. *Appl. Phys. Lett.* **2013**, *103*, 172406.

(30) Bortolotti, P.; Grimaldi, E.; Dussaux, A.; Grollier, J.; Cros, V.; Serpico, C.; Yakushiji, K.; Fukushima, A.; Kubota, H.; Matsumoto, R.; Yuasa, S. *Phys. Rev. B: Condens. Matter Mater. Phys.* **2013**, *88*, 174417.

(31) Kardasz, B.; Montoya, E. A.; Eyrich, C.; Girt, E.; Heinrich, B. *J. Appl. Phys.* **2011**, *109*, 07D337.

(32) Dutta, S.; Chang, S.-C.; Nickvash, K.; Nikonov, D. E.; Sasikanth, M.; Young, I. A.; Naeemi, A. *Sci. Rep.* **2015**, *5*, 9861.

(33) Verba, R.; Tiberkevich, V.; Slavin, A. *Appl. Phys. Lett.* **2015**, *107*, 112402.

DOI: 10.1021/acs.nanolett.6b04725
Nano Lett. 2017, 17, 572−577

(34) Khitun, A.; Bao, M.; Wang, K. L. *J. Phys. D: Appl. Phys.* **2010**, *43*, 264005.

DOI: 10.1021/acs.nanolett.6b04725
Nano Lett. 2017, 17, 572−577